

# Multiwavelength Spectral Studies Of Fermi-LAT Blazars

M. Joshi, A. Marscher, S. Jorstad  
*Boston University, Boston, MA, USA*

M. Böttcher  
*Ohio University, Athens, OH, USA*

I. Agudo  
*Boston University, Boston, MA, USA & IAA, Granada, Spain*

V. Larionov  
*St. Petersburg State University, St. Petersburg, Russia*

M. Aller  
*University of Michigan, Ann Arbor, MI, USA*

M. Gurwell  
*SAO, Cambridge, MA, USA*

A. Lähteenmäki  
*Metsähovi Radio Observatory, Kylmälä, Finland*

We present multiwavelength spectral analyses of two Fermi-LAT blazars, OJ 287 and 3C 279, that are part of the Boston University multiwaveband polarization program. The data have been compiled from observations with Fermi, Swift, RXTE, the VLBA, and various ground-based optical and radio telescopes. We simulate the dynamic spectral energy distributions (SEDs) within the framework of a multi-slice, time-dependent leptonic jet model for blazars, with radiation feedback, in the internal shock scenario. We use the physical jet parameters obtained from the VLBA monitoring to guide our modeling efforts. We discuss the role of intrinsic parameters and the interplay between synchrotron and inverse Compton radiation processes responsible for producing the resultant SEDs.

## I. INTRODUCTION

Blazar jets are highly violent in nature and are dominated by ultrarelativistic particles. The SED of blazars consists of two spectral bumps. The low-energy component is due to synchrotron radiation emanating from relativistic particles, and the high-energy component (for leptonic jet model) is a result of Compton upscattering of the seed photon field by ultrarelativistic particles. The seed photons could either be the synchrotron photons produced in the jet (synchrotron self Compton, SSC) [9, 10], and/or external disk photons entering the jet directly (external Compton disk, ECD) [1, 2], and/or the disk photons getting reprocessed in the broad line region (BLR) (external Compton cloud, ECC) [5, 11], and/or the dusty torus [3, 6] and then entering the jet. The spectral variability patterns and SEDs are important tools used for understanding the acceleration of particles and the time-dependent interplay of various radiation mechanisms responsible for the observed emission.

Here, we analyze the multiwaveband SED of two Fermi-LAT blazars, OJ287 and 3C 279, using the 1-D multi-slice time-dependent leptonic jet model, with radiation feedback scheme of [7] to gain understanding of the role of various intrinsic parameters and radia-

tion processes in producing the resultant SEDs.

We briefly describe the model of [7] in §II. We discuss our first results from this study in §III. We summarize our results and give a brief description of future work in §IV.

## II. INTERNAL SHOCK MODEL

The mode of acceleration of plasma electrons (and positrons) to highly relativistic energies and its location in the jet is still not completely understood. One way to comprehend the physics of particle acceleration is the internal shock model, in which the central engine (black hole + accretion disk) spews out shells of plasma with different velocity, mass, and energy. The collision between such shells gives rise to internal shocks (reverse (RS) and forward (FS)), which convert the ordered bulk kinetic energy of the plasma into the magnetic field energy and random kinetic energy of the particles. The highly accelerated particles then radiate and produce the emission observed from the jet.

The collision of two plasma shells results in an emission region as shown in Figure 1. The treatment of shell collision and shock propagation is hydrodynamic

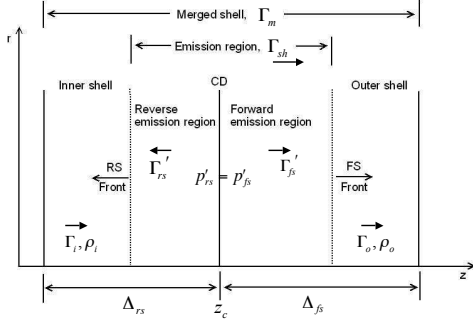


FIG. 1: Schematic of the emission region with RS traveling into the inner shell of bulk Lorentz factor (BLF)  $\Gamma_i$ , and FS moving into the outer shell of BLF with  $\Gamma_o$ , such that  $\Gamma_i > \Gamma_o$ . The primed quantities refer to the comoving frame and unprimed refer to the lab (AGN) frame. The comoving pressures  $p'_{is}$  and  $p'_{os}$  of the shocked fluids across the contact discontinuity (CD) are equal.  $\Delta_{rs}$  and  $\Delta_{fs}$  are the widths of the inner and outer shell after the collision obtained from the shock dynamics [12].

and relativistic in nature [12].

The evolution of electron and photon population inside the emission region are governed, respectively, by,

$$\frac{\partial n_e(\gamma, t)}{\partial t} = -\frac{\partial}{\partial \gamma} \left[ \left( \frac{d\gamma}{dt} \right)_{\text{loss}} n_e(\gamma, t) \right] + Q_e(\gamma, t) - \frac{n_e(\gamma, t)}{t_{e, \text{esc}}} \quad (1)$$

and

$$\frac{\partial n_{ph}(\epsilon, t)}{\partial t} = \dot{n}_{ph, \text{em}}(\epsilon, t) - \dot{n}_{ph, \text{abs}}(\epsilon, t) - \frac{n_{ph}(\epsilon, t)}{t_{ph, \text{esc}}} \quad (2)$$

Here,  $(d\gamma/dt)_{\text{loss}}$  is the radiative energy loss rate, due to synchrotron and SSC losses, for the electrons.  $Q_e(\gamma, t)$  is the sum of external injection and intrinsic  $\gamma - \gamma$  pair production rate and  $t_{e, \text{esc}}$  is the electron escape time scale.  $\dot{n}_{ph, \text{em}}(\epsilon, t)$  and  $\dot{n}_{ph, \text{abs}}(\epsilon, t)$  are the photon emission and absorption rates corresponding to the electrons' radiative losses, and  $t_{ph, \text{esc}} = (3/4)R_b/c$  is the photon escape timescale. The evolution of the electron and photon population is followed in a time-dependent manner inside the emission region and radiative energy loss rates as well as photon emissivities are calculated using the time-dependent radiation transfer code of [7].

The model follows the evolution of the emission region out to sub-pc scales and simulates only the early phase of  $\gamma$ -ray production. During this time, the radiative cooling is strongly dominant over adiabatic cooling and the emission region is highly optically thick out to GHz radio frequencies. Thus, the simulated radio flux is well below that of the actual radio data. Also, the phase of the emission region in

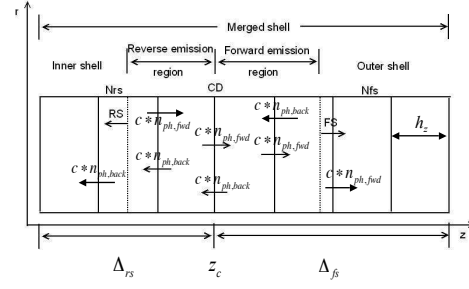


FIG. 2: Schematic of the radiative transfer in between the slices using the appropriate photon escape probability function. The unprimed  $n_{ph, \sim \text{fwd/back}}$  values represent the photon densities in the forward and backward direction, respectively, in the comoving frame of the emission region. The rest of the unprimed quantities refer to the lab frame.

which it gradually becomes transparent to radio frequencies is not simulated, as that would require the introduction of several additional, poorly constrained parameters.

### A. Multi-slice Radiation Transfer Scheme

A cylindrical emission region is considered to calculate the resultant spectrum in a time-dependent manner. The inhomogeneity in the photon and particle density throughout the emission region is realized by dividing the region into multiple slices, as shown in Figure 2.

The photon density of a zone and the probability of escape for a photon from that zone in a particular direction (forward, backward, or sideways),  $P$ , are used to calculate photon escape rates in that direction, according to

$$\frac{dn_{ph, \text{fwd/back/side}}(\epsilon, \Omega)}{dt} = \frac{n_{ph}(\epsilon, \Omega)}{t_{ph, \text{esc}}} P_{\text{fwd/back/side}} \quad (3)$$

where  $t_{ph, \text{esc}}$  is the photon escape timescale for a cylindrical region.

We use the scheme presented in equation 3 to calculate the radiation transfer within each slice and in between the slices [7].

## III. FIRST RESULTS

The time-dependent model, calculating synchrotron and SSC radiation processes, developed in [7] has been used to reproduce the observed SED of two Fermi-LAT blazars, OJ287 and 3C 279 that are part of the Boston University multiwaveband monitoring program. We have collected the data from observations with Fermi, Swift, RXTE, the VLBA, and various ground-based optical and radio telescopes to construct

the multiwaveband SEDs of OJ287, and 3C 279, the latter of which corresponds to the quasar's optical high state as observed on 15 January 2006.

OJ287 is a BL Lac object purported to have a black hole binary system [15]. The blazar has exhibited spectral and polarization variability in the past [13]. Here, we apply the model of [7] with the ECD component included (Joshi et al., 2012, in prep.) with 50 slices in the forward and 50 slices in the reverse emission regions to analyse the SED of OJ287 as observed on 10/28/2008. Figure 3 shows the instantaneous and time-integrated simulated SED of OJ287 for that day. The model independent parameters [4] estimated from the SED, VLBA observations [8], and variability on 1-day timescale were used to develop an initial set of input parameters:

$$\begin{aligned}
 \delta &\approx 16.5 \\
 R &\approx 3.5 \times 10^{15} \text{ cm} \\
 B &\approx 0.52 \epsilon_B^{2/7} \text{ G} \\
 \gamma_{\min} &\approx 1.1 \times 10^3 \\
 \gamma_{\max} &\approx 3.0 \times 10^4 \\
 q &\approx 4.2 \\
 \theta_{\text{obs}} &\approx 3.2^\circ
 \end{aligned} \tag{4}$$

Here,  $\delta$  is the Doppler boosting factor assumed to be equal to the BLF of the emission region (as estimated from VLBA observations). The symbols  $R$  &  $B$  represent the values of comoving radius and magnetic field in the emission region and  $\epsilon_B$ , which is not a part of the model of [7], is the ratio of magnetic field and electron energy density assumed to be equal to 1 here. The  $\gamma_{\min}$  &  $\gamma_{\max}$  refer to the low and high energy cutoffs of the electron energy distribution. The spectral index of the electron population is given by  $q$  and  $\theta_{\text{obs}}$  is the observing angle inferred from VLBA observations.

The initial set of parameters was modified to reproduce the state of OJ287 as observed on 10/28/2008. Table I lists the parameters used for obtaining the resultant SED of the source shown in Fig. 3. These parameters result in a  $\Gamma_{\text{sh}} \approx 16.4$  for the entire emission region,  $B \approx 5.0 \text{ G}$  and  $\gamma_{\max} \approx 1.5 \times 10^5$  for both forward and reverse emission regions, and  $\gamma_{\min, \text{fs}} \approx 5.6 \times 10^2$  &  $\gamma_{\min, \text{rs}} \approx 1.0 \times 10^3$  for forward and reverse emission regions, respectively.

As can be seen from the figure, the lower-energy bump of the time-integrated simulated SED passes very close to the IR, optical, and UV data points, indicating that the synchrotron component is responsible for this part of the jet emission. The spectral upturn takes place in the soft X-rays at  $\geq 0.14 \text{ keV}$  due to the presence of the SSC component in the simulation and the lower-energy part of the SSC component passes close to the X-ray data implying the dominance of SSC component in producing this part of the high-energy bump. The model (SSC+ECD), at this point,

underpredicts the  $\gamma$ -ray photon flux suggesting that the contribution from the BLR might play a dominant role in reproducing this emission.

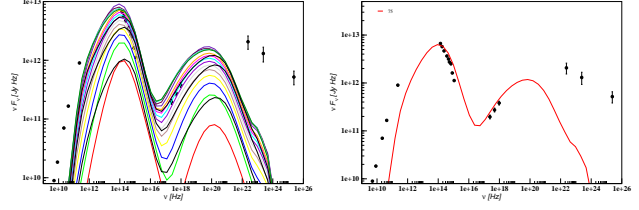


FIG. 3: Simulated instantaneous and time-integrated (averaged over 1 day) SED of OJ287 for 10/28/2008.

The flat-spectrum radio quasar (FSRQ), 3C 279, was observed in its optical high state on 01/15/2006, almost a month before it was observed by MAGIC emitting in the TeV energy regime for the first time ever [14]. Figure 4 shows the instantaneous and time-integrated simulated SED of 3C 279 for that day. The model independent parameters [4] that were estimated using the SED, VLBA observations [8], and variability on 1-day timescale were used to develop an initial set of input parameters:

$$\begin{aligned}
 \delta &\approx 15.5 \\
 R &\approx 2.5 \times 10^{16} \text{ cm} \\
 B &\approx 0.82 \epsilon_B^{2/7} \text{ G} \\
 \gamma_{\min} &\approx 9.0 \times 10^2 \\
 \gamma_{\max} &\approx 2.2 \times 10^4 \\
 q &\approx 4.3 \\
 \theta_{\text{obs}} &\approx 2.1^\circ
 \end{aligned} \tag{5}$$

All symbols refer to the same quantities as explained above and the entire emission region, as mentioned above, has been divided into 100 slices to analyze the observed SED of the source. The initial set of parameters was modified to reproduce the state of 3C 279 as observed on 01/15/2006. Table I lists the parameters used for obtaining the resultant SED of the source shown in Fig. 4. These parameters result in  $\Gamma_{\text{sh}} \approx 16.6$  for the entire emission region,  $B \approx 4.0 \text{ G}$  and  $\gamma_{\max} \approx 2.2 \times 10^5$  for both forward and reverse emission regions, and  $\gamma_{\min, \text{fs}} \approx 5.8 \times 10^2$  &  $\gamma_{\min, \text{rs}} \approx 1.3 \times 10^3$  for forward and reverse emission regions, respectively.

As can be seen from the figure, the observed SED for 01/15/2006 shows a high-energy bump that is indicative of a dominant SSC component and a suppressed EC component. The time-integrated simulated SED passes very close to the IR and optical data points, indicating that the synchrotron component responsible for the lower energy bump of the SED. The spectral upturn takes place in the soft X-rays at  $\geq 0.11 \text{ keV}$  due to the presence of the SSC component in the simulation. The lower-energy part of the SSC component

reproduces the X-ray data quite well, suggesting the dominance of SSC component in producing this part of the high-energy bump.

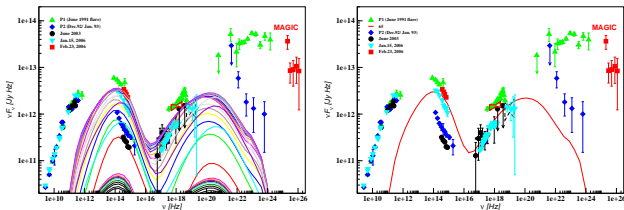


FIG. 4: Simulated instantaneous and time-integrated (averaged over 1 day) SED of 3C 279 for 01/15/2006.

TABLE I: Model parameters used to reproduce the state of OJ287 and 3C 279 as observed on 10/28/2008 & 01/15/2006, respectively.

Source	$L_w$	$\Gamma_i$	$\Gamma_o$	$q$	$\varepsilon_e$	$\varepsilon_B$	$\zeta_e$
	$[10^{47} \text{ ergs/s}]$				$[10^{-2}]$	$[10^{-3}]$	$[10^{-2}]$
3C279	5	35	10	4	9	3	2.5
OJ287	4	25	12	4.2	9	14	1.0

Source	R	$\theta_{obs}$	$L_{disk}$	$M_{BH}$	$\eta_{acc}$
	$[10^{16} \text{ cm}]$	$[\text{deg}]$	$[10^{44} \text{ ergs/s}]$	$[10^8 M_{Sol}]$	$[10^{-2}]$
3C279	3.7	2.5	-	-	-
OJ287	4.0	2.5	2	2	6

$L_w$ : luminosity of the injected electron population in the blob,  $\Gamma_{i,o}$ : BLFs of the inner and outer shells before collision,  $q$ : particle spectral index,  $\varepsilon_e$ : ratio of electron and shock energy density,  $\varepsilon_B$ : ratio of magnetic field and shock energy density,  $\zeta_e$ : fraction of accelerated electrons, R: comoving radius,  $\theta_{obs}$ : viewing angle,  $L_{disk}$ : accretion disk luminosity,  $M_{BH}$ : Mass of the BH, and  $\eta_{acc}$ : accretion efficiency

#### IV. DISCUSSION AND FUTURE WORK

The time-integrated SEDs of both OJ287 & 3C 279 need further adjustments of parameters that are listed in Table I in order to obtain a satisfactory fit. The external Compton component due to photons entering the jet from the BLR and dusty torus needs to be incorporated in the existing model of [7] to correctly reproduce the SEDs of blazars, especially for flat spectrum radio quasars (Joshi et al. 2012, in prep.).

Further, we plan to incorporate the effects of magnetic field orientation, as inferred from polarization monitoring programs, on the resultant spectral variability and SEDs of blazars. This would further aid us in the study of intrinsic parameter differences between various blazar subclasses, arising from the orientation of the magnetic field in the jet.

We plan to study the evolution of SED of blazars from quiescent to flaring state in the light of the modified time-dependent model of [7] (Joshi et al. 2012, in prep.). We will then compare the results with multi-wavelength data gathered by the Fermi-LAT and other telescopes.

#### Acknowledgments

This research was supported in part by NASA through Fermi grants NNX10AO59G, NNX08AV65G, and NNX08AV61G and ADP grant NNX08AJ64G, and by NSF grant AST-0907893.

- 
- [1] Dermer, C. D., & Schlickeiser, R., 1993, ApJ, 416, 458
  - [2] Böttcher, M., Mause, H., & Schlickeiser, R., 1997, A&A, 324, 395
  - [3] Arbeiter, C., Pohl, M., & Schlickeiser, R., 2002, A&A, 386, 415
  - [4] Böttcher, M., et al., 2005, ApJ, 631, 169
  - [5] Böttcher, M., & Bloom, S. D., 2000, AJ, 119, 469
  - [6] Blażejowski, M., et al. 2000, ApJ, 545, 107
  - [7] Joshi, M., & Böttcher, M., 2011, ApJ, 727, 21
  - [8] Jorstad, S. G., et al., 2005, AJ, 130, 1418
  - [9] Marscher, A. P., & Gear, W. K., 1985, ApJ, 298, 114
  - [10] Georganopoulos, M., & Marscher, A. P., 1998, ApJ, 506, 621
  - [11] Sikora, M., Begelman, M. C., & Rees, M. J., 1994, ApJ, 421, 153
  - [12] Spada, M., et al., 2001, MNRAS, 325, 1559
  - [13] Agudo, I., et al., 2011, ApJL, 726, 13
  - [14] Collmar, W., et al., 2010, A&A, 522, 66
  - [15] Valtonen, M. J., Lehto, H. J., & Pietilä, H., 1999, A&A, 342, L29